Title
Non-aqueous phase liquid spreading during soil vapor extraction

Journal
Journal of Contaminant Hydrology, 68(3/4/2008)

Author
Kneafsey, Timothy J.

Publication Date
2000-06-27

LBNL-46519
Preprint

ERNEST ORLANDO LAWRENCE
BERKELEY NATIONAL LABORATORY

Non-Aqueous Phase Liquid Spreading During Soil Vapor Extraction

Timothy J. Kneafsey and James R. Hunt

Earth Sciences Division

June 2000

Submitted to
Journal of
Contaminant Hydrology

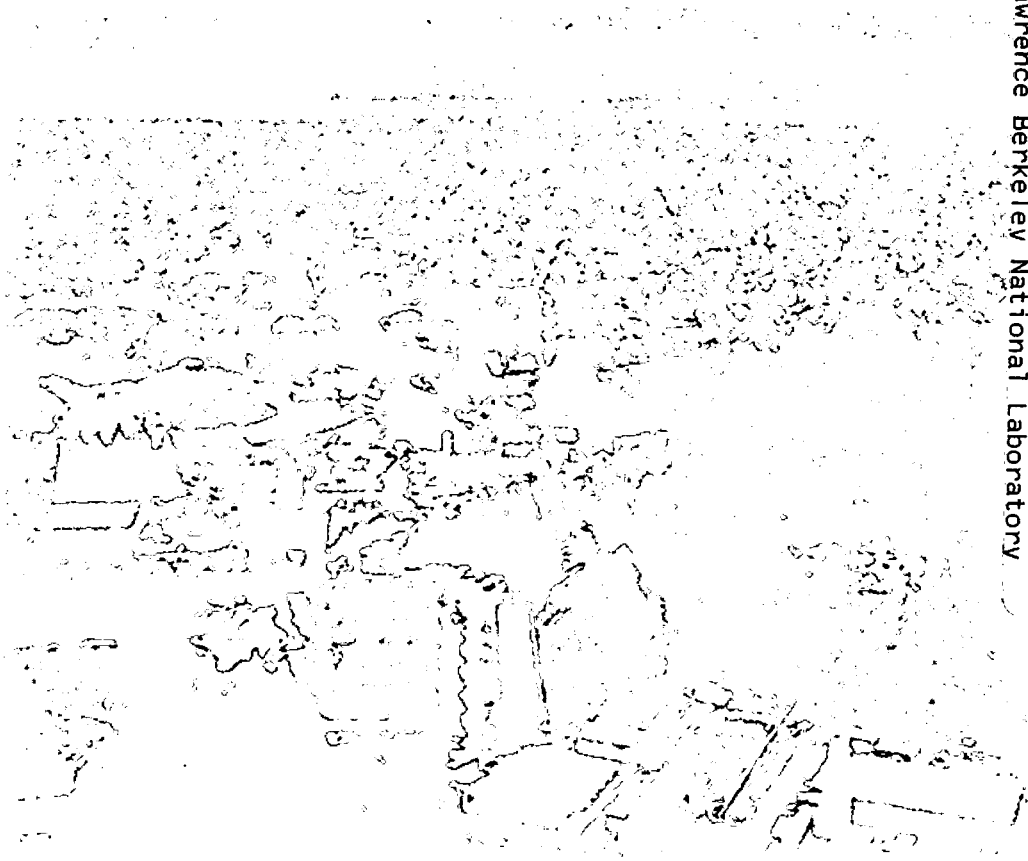

DISCLAIMER

LBNL-46519

Non-Aqueous Phase Liquid Spreading During Soil Vapor Extraction

Timothy J. Kneafsey and James R. Hunt

Earth Sciences Division
Ernest Orlando Lawrence Berkeley National Laboratory
University of California
Berkeley, California 94720

June 2000

This work was supported by the Contract NIEHS Superfund Basic Research Program under Grant No. 3P432ES04705-14 through the U.S. Department of Energy under Contract No. DE-AC03-76SF00098.

ABSTRACT

Many non-aqueous phase liquids (NAPLs) are expected to spread at the air-water interface. This spreading should increase the surface area for mass transfer and efficiency of volatile NAPL recovery by soil vapor extraction. A model is developed that couples oil film flow and vapor diffusion under conditions likely encountered during soil vapor extraction. The model predicts that spreading can enhance the recovery by factors of two to greater than ten compared to conditions where the liquid does not spread. Experiments were conducted with spreading volatile oils hexane and heptane. Within stagnant gas porous medium columns up to a meter in height, spreading was less than ten centimeters and did not contribute significantly to hexane loss by evaporation and diffusion. Water films within these columns likely prevented film spreading through water film thinning and oil film pinning.

1. INTRODUCTION

Many non-aqueous phase liquids (NAPLs) are of environmental concern when released near the earth's surface. These liquids are composed of compounds that often exhibit toxic and/or carcinogenic properties to humans and other biota and can reach target populations by drinking water or inhalation pathways. Understanding the mechanisms of NAPL migration is important to better understand their subsurface transport and to design efficient cleanup schemes. Within the vadose zone, NAPL migration is controlled by a number of processes including flow by gravitation and capillary forces, liquid spreading at air-water interfaces, and evaporation. The efficiency of NAPL recovered by soil vapor extraction is dependent on these processes. Current models for soil vapor extraction (SVE) are based on selective air flow through regions containing NAPL held at residual saturation where local equilibrium is assumed (Armstrong et al., 1994; Baehr et al., 1989; Kearl et al., 1991; Lingineni and Dhir, 1992; Massmann et al., 2000). The efficiency of SVE for NAPL floating on the water table is the focus of this research.

NAPLs in the subsurface respond to buoyant, viscous, and interfacial forces (Conrad et al., 1992). Buoyant forces cause the NAPL to move vertically up or down depending on the relative density of the NAPL and the surrounding fluid (generally water or air), viscous forces resist the movement of the NAPL in any direction, and interfacial forces direct wetting NAPLs into and non-wetting NAPLs out of small pores. Interfacial forces also cause liquids to spread in a film

or coalesce into lenses depending on the interfacial tensions among the air, water, and NAPL. NAPLs which tend to spread in the subsurface will have a greater air-NAPL surface area, which will enhance mass transfer into the soil gas (Anderson, 1994; Wilson, 1990) and soil vapor extraction efficiency.

Interfacial tensions result from the differences in attraction between like and unlike molecules. The spreading coefficient (S) for an oil phase describes the tendency of oil to spread on water in the presence of air (Adamson, 1990), and is given by

$$S = \sigma_{aw} - (\sigma_{ow} + \sigma_{oa}) \qquad (1)$$

where σ is the interfacial tension and subscripts a, w, and o refer to the air, water, and oil phases respectively, and pairs of subscripts refer to the interface between the respective phases. If S is positive, the oil spreads spontaneously; if negative, the oil beads up into lenses. For example, hexane has a reported interfacial tension of 18.4 mN/m with air and 51.1 mN/m with water (Demond and Lindner, 1993), yielding an S of 2.9 mN/m for pure water and hexane phases. Interfacial tensions are dependent upon oil and water partitioning between the two liquid phases often resulting in lower spreading coefficients after mutual saturation. The value of the initial spreading coefficient may be positive, negative or zero, but the value of the equilibrium spreading coefficient may only be zero or negative (Hirasaki, 1993); thus spreading may occur until all available surfaces are covered, or an equilibrium water-oil-air configuration is attained, at which point spreading stops. The spreading tendency of some oil mixtures on the air-water interface has been observed to change from negative to positive over time (Schroth et al., 1995). This may be due to changes in the composition of the

oil. Interfacial tensions also change with the temperature and contamination. Gradients in interfacial tension arising from disequilibrium can cause spreading, and this is called the Marangoni effect (Ahmad and Hansen, 1972).

Oil film spreading velocities may be on the order of tens of cm/s on a pool of water (Davies and Rideal, 1963). Spreading rate relations have been derived or observed for many free surface conditions (Ahmad and Hansen, 1972; Davies and Rideal, 1963; Fraaije and Cazabat, 1989; Gaver and Grotberg, 1992; Joanny, 1987). Vigorous film spreading over thin liquid substrates may cause temporary or permanent rupture of the substrate film (Ahmad and Hansen, 1972; Fraaije and Cazabat, 1989; Gaver and Grotberg, 1992). In laboratory three-phase (water-oil-air) systems in porous media and micromodels investigating contaminant transport and enhanced oil recovery, flow in films has explained rapid migration of spreading oils (Blunt et al., 1994; Kalaydjian et al., 1993; Keller et al., 1997; McBride et al., 1992; Oren and Pinczewski, 1992; Soll et al., 1993; Wilson et al., 1990). Within the vadose zone, NAPL spreading is expected and quantification of the effects of film spreading on soil vapor extraction has not been previously performed. This paper undertakes a mechanistic evaluation of film spreading during soil vapor extraction and then presents laboratory data to examine the significance of film spreading.

2. FILM SPREADING

We consider a spreading NAPL floating in a pool on the water table in which there is no air or water flow. Above the pool, NAPL is drawn upwards on the air-water interface by an imbalance in interfacial tensions in what we call a film zone. Above the film zone is the vapor diffusion zone where diffusive mass transport

dominates. The film and vapor diffusion zones are similar to the conceptual model for water evaporation through soil columns used by Gardner (1958). Flow in these two zones will be considered separately below and then combined into a coupled model.

2.1 Film Zone

An oil film with a positive spreading coefficient spreads vertically upwards over a water wet mineral surface, with the thickness of the lubricating water film and the oil film assumed to be constant (Figure 1). Water and spreading oil are assumed to be infinitely available from a pool at location z = 0. At equilibrium, the spreading force per length, S, is balanced by the gravitational force per length, $\rho_o g d_o h_{f,eq}$, providing an expression for the equilibrium film height.

$$h_{f,eq} = \frac{S}{\rho_o g d_o} \tag{2}$$

Under dynamic conditions when the film height, h_f, is less that the equilibrium height, the lubrication approximation (Denn, 1980) is used to describe liquid flow. This analysis assumes a no slip boundary at the water-solid interface (x=0), constant velocity and shear stress at the oil-water interface ($x=d_w$), and no shear stress at the oil-air interface ($x=d_w+d_o$). Under these conditions, the oil velocity (v_o) in the film is:

$$v_o(x) = -\frac{d_w^2}{2\mu_w}\left(\frac{dP_w}{dz} + \rho_w g\right) + \frac{1}{\mu_o}\left(\frac{dP_o}{dz} + \rho_o g\right)\left[\frac{x^2}{2} - (d_o + d_w)x + \frac{d_w^2}{2} + d_o d_w\left(1 - \frac{\mu_o}{\mu_w}\right)\right] \tag{3}$$

where d is the film thickness, and μ is viscosity. Averaging the oil velocity over the oil film thickness yields:

(4)

$$V_o = -\frac{d_w^2}{2\mu_w}\left(\frac{dP_w}{dz} + \rho_w g\right) - \left(\frac{dP_o}{dz} + \rho_o g\right)\left(\frac{d_o^2 + 3d_o d_w}{3\mu_o} + \frac{d_o d_w}{\mu_w}\right)$$

If hydrostatic conditions are assumed in the water film, the first term on the right hand side is dropped. At equilibrium, V_o is zero and the oil pressure gradient is hydrostatic, thus $dP_o/dz=-\rho_o g$. Using an expression for $\rho_o g$ from (2) gives an equilibrium pressure gradient in the oil of $\left.\frac{dP_o}{dz}\right|_{eq} = -\frac{S/d_o}{h_{f,eq}}$ which indicates a pressure difference of S/d_o over a length $h_{f,eq}$. Under nonequilibrium conditions, the pressure difference in the oil is the same, S/d_o, and the length is less, h_f. Thus $\frac{dP_o}{dz} = -\frac{S}{h_f d_o}$, and (4) becomes

$$V_o = \left(\frac{S}{h_f d_o} - \rho_o g\right)\left(\frac{d_o^2 + 3d_o d_w}{3\mu_o} + \frac{d_o d_w}{\mu_w}\right) \qquad (5)$$

The vertical flux of oil in films in a porous medium, F_f, is the average velocity multiplied by the specific surface area:

$$F_f = \left(\frac{S}{h_f d_o} - \rho_o g\right)\left(\frac{d_o^2 + 3d_o d_w}{3\mu_o} + \frac{d_o d_w}{\mu_w}\right)\phi\rho_o d_o \qquad (6)$$

where ϕ is the specific surface area of the air-water interface (surface area per volume), approximated by the solid specific interfacial area. For monodisperse spheres, this is $3(1-n)/r_g$ where n is the porosity and r_g is the grain radius.

2.2 Vapor Diffusion Zone

In the vapor diffusion zone, the flux of volatile oil occurs by diffusion. Here we assume a two component gas phase containing the component of interest and air. Fick's law is $F_A = -C_{tot} D_{AB} \frac{dy_A}{dx}$ where F_A is the molar flux of compound A, C_{tot} is the total gas concentration ($C_{tot} = P_{tot}/RT$) where P_{tot} is the total pressure, R is the gas constant, and T is absolute temperature, D_{AB} is the diffusion coefficient of compound A in the binary AB system, and y_A is the mole fraction of compound A in the gas phase. This formulation is not sufficient when mole fractions are high. Under that condition, the flux equation that accounts for diffusive and bulk fluxes is (Welty et al., 1984)

$$F_A = -C_{tot} D_{AB} \frac{dy_A}{dx} + y_A (F_A + F_B) \tag{7}$$

where F_B is the flux of B (i.e. air). When concentrations are dilute and advective fluxes low, this reduces to Fick's law. In a porous medium, diffusive flux is reduced by the presence of solid particles and liquids and a longer path due to tortuosity. The diffusion coefficient in a porous medium can be corrected using the Millington-Quirk relationship (Jury et al., 1991):

$$D_{AB,pm} = \frac{n_a^{10/3}}{n^2} D_{AB} \tag{8}$$

where n_a is the air-filled porosity.

For passive soil vapor loss for liquid oil having saturated vapor (y_{sat} -saturated gas phase mole fraction) at the bottom and zero contaminant in the air at the surface

through a soil of thickness h_v, the steady-state gas flux can be determined from the solution to (7) assuming negligible air motion, F_B=0, or

$$F_v = \frac{C_{tot} D_{AB,pm}}{h_v} \ln\left(\frac{1}{1-y_{sat}}\right) \quad (9)$$

2.3 Coupled Model

For the case where there is no advective transport of soil gas, there will be a balance between film flow and vapor diffusion at steady state. For this one-dimensional system, the oil film flux, F_f, in Equation (6) must be equal to the volatile flux, F_v, in Equation (9). This steady-state condition determines the heights of the film and vapor zones. This coupled model is demonstrated for hexane as the oil using various properties listed in Table 1.

This coupled model is evaluated in Figure 2 for vadose zone thicknesses of 100, 10, and 1 m (2a, 2b, and 2c, respectively). In all three cases, the oil film height is plotted against assumed water film thicknesses. At equilibrium, the oil film height is 6.4 meters. For the 100 m thick vadose zone in 2a, vapor diffusion through the soil is limiting the flux and the oil film is always close to the equilibrium height for any porous medium grain size. In Figure 2b, where the vadose zone is 10 m thick, the film height for the finest porous medium (r_g=10^{-5}m) is always at equilibrium given the high specific surface area of the air-water interface that permits film flow. The film heights for r_g=10^{-5}m are only defined up to a water film thickness of 10^{-6} m. Greater water film thicknesses would not permit a continuous air-water interface to be available for film flow. As the thickness of the stagnant water film increases, film flow becomes more important because thicker water films provide greater lubrication for oil film flow. For the

shallowest vadose zone in Figure 2c that is less than the equilibrium height, the actual film height is again greatest for the smallest porous medium grain size and increases with water film thickness.

2.4 Extension to Soil Vapor Extraction

In soil vapor extraction, air is drawn through a region containing a volatile contaminant which will enhance evaporation over passive transport considered earlier. Gas-phase concentrations in the extracted air downstream of a lens of oil on the water table are compared for a spreading and a nonspreading oil as illustrated in Figures 3a and 3b. Horizontal soil gas transport and vertical diffusion through a uniform porous medium is described by:

$$U_x \frac{\partial C}{\partial x} = D_z \frac{\partial^2 C}{\partial z^2} \qquad \textbf{(10)}$$

where U_x is the horizontal air approach velocity, C is the gas-phase concentration of the oil, and D_z is the transverse dispersion coefficient, defined as:

$$D_z = D_{AB,pm} + \alpha \frac{U_x}{n_a} \qquad \textbf{(11)}$$

where α is the dispersivity.

The boundary conditions for a nonspreading oil are a zero inlet concentration at x = 0, the gas-phase concentration immediately above the oil pool is saturated, and there is no source or sink of oil as z approaches ∞. Under these conditions, the average concentration of soil-vapor extracted at a distance L for non-spreading oil, $C_{avg,ns}(L)$, is (Hunt et al., 1988; Hunt et al., 1989):

$$C_{avg,ns}(L) = C_{sat}\left\{erfc(\omega) + \frac{1-\exp(-\omega^2)}{\omega\sqrt{\pi}}\right\} \quad (12)$$

where

$$\omega = \frac{H}{2(D_z L/U_x)^{1/2}} \quad (13)$$

and H is the thickness of the unsaturated zone. The variable ω compares the vadose zone thickness to the vertical diffusion distance in the contact time available.

In the case of a spreading oil with a film height of h_f, the gas-phase concentration is expected to be C_{sat} within the film zone. The average concentration in the extracted air is then:

$$C_{avg,s} = \frac{C_{sat}}{\omega}\left((\omega-\omega_f)erfc(\omega-\omega_f) + \frac{1-\exp\left[-(\omega-\omega_f)^2\right]}{\sqrt{\pi}} + \omega_f\right) \quad (14)$$

where

$$\omega_f = \frac{h_f}{2(D_z L/U_x)^{1/2}} \quad (15)$$

The ratio of the spreading to the nonspreading concentration is an enhancement factor, η, which from Equations (12) and (14) gives,

$$\eta = \frac{\omega_f + (\omega - \omega_f)erfc(\omega - \omega_f) + \frac{1}{\sqrt{\pi}}\left\{1 - \exp\left[-(\omega - \omega_f)^2\right]\right\}}{\omega erfc(\omega) + \frac{1}{\sqrt{\pi}}\left\{1 - \exp\left[-\omega^2\right]\right\}} \quad (16)$$

This model for the influence of spreading on SVE was evaluated for hexane as a function of vadose zone height, porous medium grain size, and water film thickness. Figure 4 considers the situation where there is only molecular diffusion (α=0) and vadose zone thicknesses of 100, 10, and 1 m. The air approach velocity (U_x) is 1 m/d and the horizontal extent of NAPL contamination (L) is 20 m. For H = 100 and 10 m vadose zones, the enhancement at low water film thicknesses is in the range of 2 to 5 but increases substantially as the water film thickness approaches the limit of one tenth the grain size. This increase is due to the greater lubrication of the thicker water films. In the case of the 1 m thick vadose zone simulated in Figure 4c, there is little enhancement caused by spreading since soil gas is expected to be nearly saturated under both spreading and nonspreading conditions.

When transverse hydrodynamic dispersion is considered in Figure 5 with α = 0.039 m (Freyberg, 1986), significantly reduced enhancement by spreading is predicted. For 100 and 10 m thick vadose zones (5a and 5b), the enhancement factor is in the range of 2 to 5, increasing as the water film thickness increases. The decrease in enhancement factors as water films approach the maximum thickness reflects increased transverse dispersion as the air-filled porosity is reduced and the gas approach velocity is held constant resulting in increased gas velocity and dispersion in the pore space. Figure 5c shows that there is no enhancement for shallow vadose zones because near-saturation conditions are achieved with and without spreading.

The models in Equations (12) and (14) for spreading and nonspreading conditions both assumed diffusion into a semi-infinite porous medium. This assumption is reasonable for thick vadose zones but only approximate as the vadose zone thickness approaches the characteristic distance for diffusion in the advection time available, that is $(2DL/U)^{1/2}$ = 1.9 m here.

From this analysis, we observe that film spreading will strongly increase soil vapor extraction efficiency in cases where the water films are thick, where the soil vapor is moving slowly, and in thicker vadose zones. In practical situations, thicker water films will be found near the water table. Slower soil vapor velocities would be expected at greater distance from soil vapor extraction wells, and also closer to the water table where increased water content reduces vapor velocity.

3. EXPERIMENTAL INVESTIGATION

Given the assumptions needed in modeling the effect of oil spreading on soil vapor extraction, an experimental investigation of film spreading in water-wet porous media was undertaken. Small-scale visualization experiments were combined with larger scale, more quantitative experiments to evaluate oil film dynamics.

3.1 Small-Scale Experiments

3.1.1 Oil Spreading Verification

To verify oil spreading on flat air-water interfaces, drops of hexane were introduced into water in petri dishes oriented horizontally. Hexane, with a positive initial spreading coefficient of 2.9 mN/m, spread horizontally in a vigorous manner, and on thin (mm-scale) water films, the water film thinned and ruptured. Following evaporation of the oil, the glass became water wet again.

3.1.2 Effect of Moisture Content

The effect of moisture content and thus water film thickness was investigated by introducing 0.3 milliliters of red dyed heptane (S = 2.7 mN/m, calculated from Demond and Lindner (1993)), into test tubes containing ~375 micron glass beads (Cataphote, Jackson Mississippi). Moisture contents ranged from 0.0002 $g_{water}/g_{dry\ glass}$ (air dry) to 0.0816. The tubes were sealed with cork stoppers covered with Teflon. A needle was used to inject the oil through the cork resulting in a small hole through the stopper. In the driest sample, a pink region formed around the liquid pool after about 30 minutes. After about 20 hours, a band of dull red dye, indicating dry dye without heptane, was observed towards the cork end of the tube about 0.5 cm from the liquid pool location. This band became more intensely colored over time indicating that liquid heptane was being transported from the liquid pool to this location where evaporation occurred. With moisture contents from 0.0049 to 0.0197, very little detectable heptane movement was observed over the course of a week. With moisture contents from 0.0274 to 0.0816, heptane movement was immediately observable with velocities on the order of centimeters per hour and the velocities increased with increasing moisture content. Thus, two thresholds were observed; slow heptane spreading

below moisture contents of 0.0049 and rapid spreading above moisture contents of 0.0274. At the lowest moisture contents, heptane is probably spreading on the solid glass surface. At intermediate water contents, heptane may have initially spread on the water film, causing water film rupture, and hindering further spreading. At the higher moisture contents, heptane was probably spreading on continuous water films. Pendular rings in a bed of spheres join at water contents of approximately 0.035 to 0.07 (Haines, 1926). Film spreading on these joined pendular rings at higher water contents may be responsible for the behavior observed.

3.1.3 Capillary Tubes

To simplify the geometry, film spreading and vapor diffusion were examined in three separate capillary tubes. Three clean 1 mm square tubes with 0.05 mm corner radii were used. Tube 1 was first filled with water and drained partially. Hexane was injected from below through a needle extending through the water, then the bottom was plugged. This initial emplacement allowed an oil film to form by spreading at the air-water interface. In Tube 2, hexane was added at the top of a water-filled tube as the water partially drained from the bottom, and this formed a drainage film. In Tube 3, Hexane was placed into the bottom of a dry tube with a long needle. Moistened air was swept across the tops of Tubes 1 and 2 to prevent water loss, and dry air was swept over Tube 3. Liquid water and hexane levels were measured for several hundred hours. The distance from the top of the tubes to the hexane and water interfaces increased with time (Kneafsey, 1996). Hexane loss was expected through a combination of film flow and vapor diffusion, and for these quasi-steady-state conditions in which the liquid level changed at a slow rate compared to the characteristic time for diffusion for the tube, liquid loss equaled vapor diffusion.

$$\frac{\rho_H}{M_H}\frac{dh_{obs}}{dt} = \frac{D_{Ha}C_t}{h_v}\ln\left(\frac{1}{1-y_{sat}}\right) \qquad (17)$$

where ρ_H is the liquid density of hexane, M_H is molecular weight of hexane, h_{obs} is the thickness of the hexane pool, D_{Ha} is the molecular diffusivity of hexane in air, and h_v is the thickness of the vapor diffusion zone. The vapor diffusion zone is determined using Equation (17) and the film zone thickness is taken as the distance from the top of the tube to the top of the liquid hexane minus the vapor diffusion zone thickness. Measured distance to interface data and film heights calculated from the data are shown in Figure 6. The slope of the measured distance to interface over time is equal to $-dh_{obs}/dt$ in Equation (17). All three tubes had a constant loss of hexane liquid which translated into a steadily increasing film height. The drainage film in Tube 2 was the largest and the spreading-formed film in Tube 1 was the smallest. It is apparent that the top of films became pinned at particular locations in the three tubes.

3.2 Large-Scale Column Experiments

To evaluate film spreading on a larger scale, experiments were conducted in meter-tall columns. The vadose zone was modeled with glass beads or sand and hexane was used as the spreading volatile oil phase. The experimental apparatus is shown in Figure 7 and consists of a tube 3.4 cm in diameter, packed with approximately 100 cm of porous medium. The columns were wetted by filling with water from the bottom and then allowing the water to drain over several days, leaving a water saturated zone at the bottom. Hexane was introduced above the water-saturated zone either at a constant head with a Mariotte bottle or at a

constant loading rate with a syringe pump. In both methods of hexane introduction, an oil zone was eventually observed above the water-saturated zone and above that oil zone is where film spreading would likely occur. Above the film zone is the vapor diffusion zone. Table 2 provides a summary of conditions and results for the 6 experiments conducted in the meter-tall columns.

In Experiments 1, 2 and 3, sweep gas was introduced at three separate locations (A, B, and C) designated in Figure 7. The nitrogen sweep gas was conditioned by saturating with water vapor at the same temperature as the columns in order to prevent changes in water content within the column. Location A had the sweep gas introduced near the bottom of the porous medium column to simulate a shallow vadose zone, location B was at an intermediate height and location C has the sweep gas flushed across the top of the porous media. In Experiments 4, 5, and 6, the sweep gas was only introduced across the top of the porous medium at location C. Hexane flux out of the columns was determined from measurements of the effluent concentration and effluent flow rate. Additionally, after reaching steady-state conditions when sweep air was introduced at location C, soil gas hexane measurements were taken from locations A and B to determine the profile of hexane within the porous media column. Gas samples were withdrawn first from location C, then B, and then from A to minimize disruption of the concentration profiles. The sampling tube was flushed out by wasting a volume equivalent to greater than three times the sampling tube volume (1.4 to 2.0 ml). Hexane was quantified by direct injection of gas into a gas chromatograph. Column temperatures were controlled to within a few degrees Celsius. Steady state conditions were defined as 1) a period exceeding the predicted time to reach 99% of steady state, 2) no apparent trend in the data, and 3) the standard deviation of the collected data was generally less than 5% of the

average. At the end of each experiment, moisture contents were determined gravimetrically while any liquid hexane was lost by evaporation. For Experiments 4 and 5, liquid hexane was introduced at a steady rate by a syringe pump at a flux approximately double the flux predicted if hexane did not spread. Additional details on materials, assembly, sampling, cleaning, and calibration are found in Kneafsey (1996).

3.2.1 Film Height Determination

The top of the oil zone was observable and thus the distance from that height to the height where sweep air was introduced represents the sum of the film zone and the vapor diffusion zone. The height of the vapor diffusion zone was quantified by two different methods: the Effluent Method and the Profile Method, and then the film height was determined by difference.

Effluent Method. Solving the mass flux equation (Eq. 7) for the hexane profile, assuming negligible air flux, F_B, the height of the vapor diffusion zone becomes

$$h_v = \frac{D_{Ha,pm} C_{tot}}{F_H} \ln\left(\frac{1-y_{H,e}}{1-y_{H,sat}}\right) \qquad (18)$$

where $y_{H,e}$ is the measured effluent hexane mole fraction, $y_{H,sat}$, is the saturated hexane mole fraction, and F_H is the hexane flux determined from the sweep gas flow rate and effluent hexane concentration.

The diffusion coefficient for each column was determined by measuring either octane (Experiments 1, 2, and 3) or hexane (Experiments 4, 5, and 6) diffusive

fluxes without water present. The method of Fuller (Reid et al., 1987) was used to estimate hexane diffusivities from the octane data. The hexane diffusion coefficient in the wetted columns was estimated by the Millington-Quirk relationship using measurements of moisture content throughout the columns (Eq. 8). For variable water contents, each moisture content measurement was applied over the region halfway up and halfway down to the next measurement, and the overall correction was made applying conductances in series.

Profile Method. Nearly linear mole fraction profiles would be expected for hexane in soils with constant moisture content (Baehr and Brueli, 1990). In the Profile Method, the gas-phase hexane mole fraction was measured at locations A and B within the column and in the column effluent. The top of the film zone was assumed to have the gas-phase mole fraction of hexane at saturation. The mole fractions were plotted with depth and a line was fitted to the data using linear regression. The line was extrapolated to the saturated mole fraction, which is assumed to be at the top of the film zone. The film zone height was then determined as the distance between the oil zone and the top of the film zone. Two separate profiles were determined in Experiments 1, 2, and 3; and three profiles were determined in Experiments 4, 5, and 6.

3.2.2 Results

The large-scale columns reached steady-state after times of 50 to 500 hours. One example of the effluent gas measurements is given in Figure 8 for Experiment 5. Over the first 150 hours, there was an increasing hexane flux as the system reached the steady-state flux of 1.59×10^{-9} mol/cm^{2}s over the time interval of 175 - 300 hours. The imposed hexane flux into the column bottom was 4.5×10^{-9} mol/cm^{2}s which is greater than the steady-state diffusive flux. While some liquid

hexane would be accumulating in the column, the difference in flux only represents a liquid accumulation velocity of about $4x10^{-3}$ cm/hr, thus a steady-state analysis is justified. In Experiments 1, 2, and 3, the time to reach steady state was approximately 100 hours when gas was swept across the top of the column at location C, and less than 50 hours when air was introduced at locations A and B. For experiment 1a, steady-state was not achieved over a 200 hour period.

Steady-state effluent concentrations were used to determine diffusive fluxes and then film heights by differences. These film heights are given in Table 2 and indicate only three experiments (1c, 4, and 6) where the film height was substantially and significantly greater than zero. The standard deviations presented incorporate the error in measuring the diffusion coefficients and the error in the flux measurements. In Experiments 1c and 6, the height of the hexane saturated zone was high and difficult to determine. Thus, the effluent method for determining film heights did not in general indicate film heights that would alter hexane flux through the column.

When gas was swept across the top of the columns (location C), hexane profiles within the columns were used to determine film heights by the Profile Method. Figure 9 plots hexane mole fractions in the gas phase and water saturation as a function of depth for the six experiments. Replicate and triplicate measurements of the hexane profiles show near-linear behavior and good reproducibility. The replicates in Experiments 1, 2, and 3 were taken one day apart, and the profiles for Experiments 4, 5, and 6 were over 7-10 days. In experiments 1 and 6, the water contents were not uniform with depth unlike the other experiments. Film heights determined by the Profile Method are indicated in the last column of Table 2. The Profile Method was only possible for Experiments 1, 2, and 3 when

the sweep air was in Configuration C. The Profile Method only gave nonzero film heights in Experiment 5 where the film height was estimated to be 17.5±3.1 cm. Substantial uncertainty in determining the film height arises from subtracting two comparable heights.

4. DISCUSSION

The possible importance of NAPL film spreading during SVE was investigated through an analysis of interfacial processes, models for microscale film spreading and for macroscale soil gas transport, and experimental measurements at small and intermediate scales. The overall analysis addresses the issue of NAPL spreading and film flow that has not been adequately addressed in the analysis of SVE for remediating volatile NAPLs in the vadose zone. Oil spreading at the air-water interface has received considerable attention by researchers, and spreading is expected under nonequilibrium conditions. As NAPL components and water tend towards chemical equilibrium, there is a reduction in the spreading coefficient.

Under positive spreading coefficient conditions, oil films are predicted to have heights on the order of a meter. Such film heights can significantly alter the efficiency of soil vapor extraction for the removal of a NAPL pool floating on the water table. An analytical model for horizontal advection and vertical diffusion predicted that spreading oils could be removed at rates 2 to 5 times faster than nonspreading oils for vadose zones 10 m and greater in thickness. Uncertainties arose in these model predictions related to water and oil film thicknesses.

To partially test these mechanistic analyses and model predictions, small and intermediate-scale experiments within idealized porous media were conducted. Hexane and heptane were adopted as volatile and spreading liquids for these experiments. In sand at variable moisture contents, heptane was observed to spread under low and high water content conditions, but not at intermediate contents. Thin water films were likely ruptured at intermediate water contents and that limited NAPL spreading. NAPL loss from simple capillary tubes also demonstrated the formation of a NAPL-solid contact line that was maintained as the NAPL evaporated and the film height extended.

Within the meter-long columns containing initially water-wet media, little or no hexane spreading was observed within the uncertainties of the experimental system. The experimental data were best described by hexane evaporation from a pool floating on the water table and no significant film zone. Multiple methods of analysis supported this observation that hexane volatilization was not enhanced by film zones. The experimental methods were capable of determining film zones greater than 10 cm in height. The lack of film spreading in these meter-tall columns is probably caused by intermediate water contents providing thin water films which thinned and possible ruptured by the hexane spreading. For Experiments 1 and 4, the larger water contents observed would be expected for smaller grain diameters with more pendular structures and higher surface area, and rough grains having indentations which will hold capillary water. In Experiment 1, due to the greater surface area, the water film thickness may be no thicker than for the larger grain diameter even though the moisture content was higher. In Experiment 4, even though the rough grains hold water in indentations, protrusions from their surface would tend to have much thinner water films which would tend to control in the case of water film rupture.

While spreading was expected to be important during SVE of volatile NAPLs, the intermediate-scale experimental results suggest that film heights will not be significant. Experiments were limited to porous media having water drained to a residual saturation and no net movement of soil gas. It is possible that oil spreading on porous media could occur in the driest porous media, but those are rather specialized conditions. These results do suggest that a combination of mechanistic analysis, idealized modeling, and laboratory experiments were needed to arrive at this conclusion. There may be additional information provided by micromodel studies, but quantitative scaling relationships of residual water, water film dynamics, porous medium grain sizes, and NAPL spreading coefficient will need to be established.

ACKNOWLEDGMENTS

This research was supported by the NIEHS Superfund Basic Research Program, grant 3P432 ES04705-14. Discussions with Clay Radke were very much appreciated. Bruce Jacobson provided necessary and timely assistance in equipment assembly. Reviews and comments by Curt Oldenburg and Andre Unger were most appreciated.

REFERENCES

Adamson, A. W., *Physical Chemistry of Surfaces*, John Wiley and Sons, Inc., 1990.

Ahmad, J., and Hansen, R. S., A Simple Quantitative Treatment of the Spreading of Monolayers on Thin Liquid Films, *Journal of Colloid and Interface Science, 38*, pp. 601 - 604, 1972.

Anderson, M. A., Interfacial Tension-Induced Transport of Nonaqueous Phase Liquids in Model Aquifer Systems, *Water, Air, and Soil Pollution, 75*, pp. 51 - 60, 1994.

Armstrong, J. E., Frind, E. O., and McClellan, R. D., Nonequilibrium Mass Transfer between the Vapor, Aqueous, and Solid Phases in Unsaturated Soils during Vapor Extraction, *Water Resources Research, 30*, pp. 355 - 368, 1994.

Baehr, A. L., and Bruell, C. J., Application of the Stefan-Maxwell Equations to Determine Limitations of Fick's Law when Modeling Organic Vapor Transport in Sand Columns, *Water Resources Research, 26*, pp. 1155 - 1163, 1990.

Baehr, A. L., Hoag, G. E., and Marley, M. C., Removing Volatile Contaminants from the Unsaturated Zone by Inducing Advective Air-Phase Transport, *Journal of Contaminant Hydrology, 4*, pp. 1 - 26, 1989.

Blunt, M., Fenwick, D., and Zhou, D., What Determines Residual Oil Saturation in Three-Phase Flow, 1994 Improved Oil Recovery Symposium, Tulsa, Oklahoma, 1994.

Conrad, S. H., Wilson, J. L., Mason, W. R., and Peplinski, W. J., Visualization of Residual Organic Liquid Trapped in Aquifers, *Water Resources Research, 28*, pp. 467 - 478, 1992.

Daubert, T. E., *Chemical Engineering Thermodynamics*, McGraw-Hill Book Company, New York, 1985.

Davies, J. T., and Rideal, E. K., *Interfacial Phenomena*, Academic Press, New York, 1963.

Del Cerro, C., and Jameson, G. J., The Behavior of Pentane, Hexane, and Heptane on Water, *Journal of Colloid and Interface Science, 78*, pp. 362 - 375, 1980.

Demond, A. H., and Lindner, A. S., Estimation of Interfacial Tension between Organic Liquids and Water, *Environmental Science and Technology, 27*, pp. 2318 - 2331, 1993.

Denn, M. M., *Process Fluid Mechanics*, Prentice-Hall, 1980.

Department of Transportation, U. S., and Coast Guard, U. S., CHRIS Hazardous Chemical Data, *Commandant Instruction M16465.15A*, 1984.

Fraaije, J. G. E. M., and Cazabat, A. M., Dynamics of Spreading on a Liquid Substrate, *Journal of Colloid and Interface Science, 133*, pp. 452 - 460, 1989.

Freyberg, D. L., A Natural Gradient Experiment on Solute Transport in a Sand Aquifer 2. Spatial Moments and the Advection and Dispersion of Nonreactive Tracers, *Water Resources Research, 22*, pp. 2031 - 2046, 1986.

Gardner, W. R., Some Steady-State Solutions of the Unsaturated Moisture Flow Equation with Applications to Evaporation from a Water Table, *Soil Science, 85*, pp. 228 - 232, 1958.

Gaver, D. P. I., and Grotberg, J. B., Droplet Spreading on a Viscous Film, *Journal of Fluid Mechanics, 235*, pp. 399 - 414, 1992.

Haines, W. B., *Journal of Agricultural Science, 15*, pp. 529-535, 1926.

Hirasaki, G. J., Structural Interactions in the Wetting and Spreading of van der Waals Fluids, *Journal of Adhesion Science Technology, 7*, pp. 285 - 322, 1993.

Hunt, J. R., Sitar, N., and Udell, K. S., Nonaqueous Phase Liquid Transport and Cleanup 1. Analysis of Mechanisms, *Water Resources Research, 24*, pp. 1247 - 1258, 1988.

Hunt, J. R., Sitar, N., and Udell, K. S., Correction to "Nonaqueous Phase Liquid Transport and Cleanup 1. Analysis and Mechanisms", *Water Resources Research, 25*, p. 1450, 1989.

Joanny, J.-F., Wetting of a Liquid Substrate, *Physico-Chemical Hydrodynamics, 9*, pp. 183 - 196, 1987.

Jury, W. A., Gardner, W. R., and Gardner, W. H., *Soil Physics*, John Wiley and Sons, Inc., 1991.

Kalaydjian, F. J.-M., Moulu, J.-C., Vizika, O., and Munkerud, P. K., Three-Phase Flow in Water-Wet Porous Media: Determination of Gas/Oil Relative Permeabilities Under Various Spreading Conditions, 68th Annual Conference and Exhibition of the Society of Petroleum Engineers, Houston, Texas, 1993.

Kearl, P. M., Korte, N. E., Gleason, T. A., and Beale, J. S., Vapor Extraction Experiments with Laboratory Soil Columns: Implications for Field Programs, *Waste Management, 11*, pp. 231 - 239, 1991.

Keller, A. A., Blunt, M. J., and Roberts, P. V., Micromodel Observation of the Role of Oil Layers in Three-Phase Flow, *Transport in Porous Media, 26*, pp. 277 - 297, 1997.

Kneafsey, T. J., The Effect of Vertical Non-Aqueous Phase Liquid Film Flow on Soil Vapor Extraction, Ph.D. dissertation, University of California, Berkeley, Berkeley, California, 1996.

Lide, D. R., *CRC Handbook of Chemistry and Physics*, , 1990.

Lingineni, S., and Dhir, V. K., Modeling of Soil Venting Processes to Remediate Unsaturated Soils, *Journal of Environmental Engineering, 118*, pp. 135 - 152, 1992.

Massmann, J., Shock, S., and Johannesen, L., Uncertainties in cleanup times for soil vapor extraction, *Water Resources Research, 36*, pp. 679-692, 2000.

McBride, J. F., Simmons, C. S., and Cary, J. W., Interfacial Spreading Effects on One-Dimensional Organic Liquid Imbibition in Water-Wetted Porous Media, *Journal of Contaminant Hydrology, 11*, pp. 1 - 25, 1992.

Oren, P. E., and Pinczewski, W. V., The Effect of Wettability and Spreading Coefficients on the Recovery of Waterflood Residual Oil by Miscible Gasflooding, 67th Annual Technical Conference and Exhibition of the Society of Petroleum Engineers, Washington, D.C., 1992.

Reid, R. C., Prausnitz, J. M., and Poling, B. E., *The Properties of Gases and Liquids*, McGraw-Hill, New York, 1987.

Schroth, M. H., Istok, J. D., Ahearn, S. J., and Selker, J. S., Geometry and Position of Light Nonaqueous-Phase Liquid Lenses in Water-Wetted Porous Media, *Journal of Contaminant Hydrology, 19*, pp. 269 - 287, 1995.

Soll, W. E., Celia, M. A., and Wilson, J. L., Micromodel Studies of Three-Fluid Porous Media Systems: Pore-Scale Processes Relating to Capillary Pressure-Saturation Relationships, *Water Resources Research, 29*, pp. 2963 - 2974, 1993.

Welty, J. R., Wicks, C. E., and Wilson, R. E., *Fundamentals of Momentum, Heat, and Mass Transfer*, John Wiley and Sons, New York, 1984.

Wilson, J. L., Pore scale behavior of spreading and non-spreading organic liquids in the vadose zone, International Conference on Subsurface Contamination by Immiscible Fluids, Calgary, Canada, 1990.

Wilson, J. L., Conrad, S. H., Mason, W. R., Peplinski, W., and Hagan, E., *Laboratory Investigation of Residual Liquid Organics from Spills, Leaks, and the Disposal of Hazardous Wastes in Groundwater*, U.S.E.P.A., Ada, Oklahoma, 1990.

Yaws, C. L., *Handbook of Transport Property Data, Viscosity, Thermal Conductivity, and Diffusion Coefficients of Liquids and Gases*, Gulf Publishing Company, 1995.

Table 1. Parameters for simulating hexane transport by film flow and vapor diffusion in porous media.

Parameter	Value	Reference
Hexane Density (ρ_o)	656 [kg/m^3]	Lide (1990)
Hexane Viscosity (μ_o)	0.000312 [Pa·s]	Department of Transportation and Coast Guard (1984)
Water Viscosity (μ_w)	0.000993 [Pa·s]	Welty et al. (1984)
Porosity (n)	0.37	Estimated
Spreading Coefficient (S)	2.9 [mN/m]	Demond and Lindner (1993)
Hexane-Air Interfacial Tension (σ_{oa})	18.4 [mN/m]	Demond and Lindner (1993)
Hexane Film Thickness (d_o)	$7x10^{-8}$ [m]	Del Cerro and Jameson (1980)
Diffusion Coefficient (D_{AB}, $D_{AB,pm}$)	$7.32x10^{-6}$ [m^2/s]	Yaws (1995)
Saturated Gas-Phase Mole Fraction (y_{sat})	0.20	Calculated from Daubert (1985)

Table 2. Experimental conditions and results for meter-tall columns.

Experiment/ Medium		Observed Partially Saturated Zone Height h_{ps} (cm)	Time to Steady State (hr)	F_H (mol/ cm^2 s)	$D_{Ha,pm}$ estimated (cm^2/ s)	Effluent Method Film Height (cm)	Profile Method Film Height (cm)
1 A	115 µm glass	19.5	>200	**	0.0061 ± 0.0002	**	
B		47.1	50	$2.0 \pm 0.1 \times 10^{-09}$	0.0106 ± 0.0005	4 ± 3	
C		76.2	100	$1.5 \pm 0.1 \times 10^{-09}$	0.0116 ± 0.0005	14 ± 5	***
2 A	770 µm glass	27	50	$5.8 \pm 0.4 \times 10^{-09}$	0.0157 ± 0.0004	5 ± 2	
B		57.9	50	$2.7 \pm 0.1 \times 10^{-09}$	0.0204 ± 0.0012	-2 ± 4	
C		93	100	$1.8 \pm 0.1 \times 10^{-09}$	0.0205 ± 0.0010	1 ± 7	***
3 A	2000 µm glass	27	50	$6.2 \pm 0.3 \times 10^{-09}$	0.0173 ± 0.0010	5 ± 2	
B		59.5	50	$2.8 \pm 0.1 \times 10^{-09}$	0.0196 ± 0.0009	4 ± 3	
C		93.7	100	$1.9 \pm 0.1 \times 10^{-09}$	0.0199 ± 0.0008	6 ± 6	1.5 ± 3.5
4*	425 - 495 µm sand	93.5	200	$1.3 \pm 0.02 \times 10^{-09}$	0.0127 ± 0.0010	13 ± 7	***
5*	375 µm glass	96.5	200	$1.6 \pm 0.04 \times 10^{-09}$	0.0181 ± 0.0008	3 ± 5	17.5 ± 3.1
6	375 µm glass	93	600	$1.6 \pm 0.1 \times 10^{-09}$	0.0132 ± 0.0006	25 ± 5	***

* Hexane injected by syringe pump at 3.5×10^{-8} mol/s (4.5×10^{-9} mol/cm^2s).

** Not at steady state.

*** Zero or negative film height calculated.

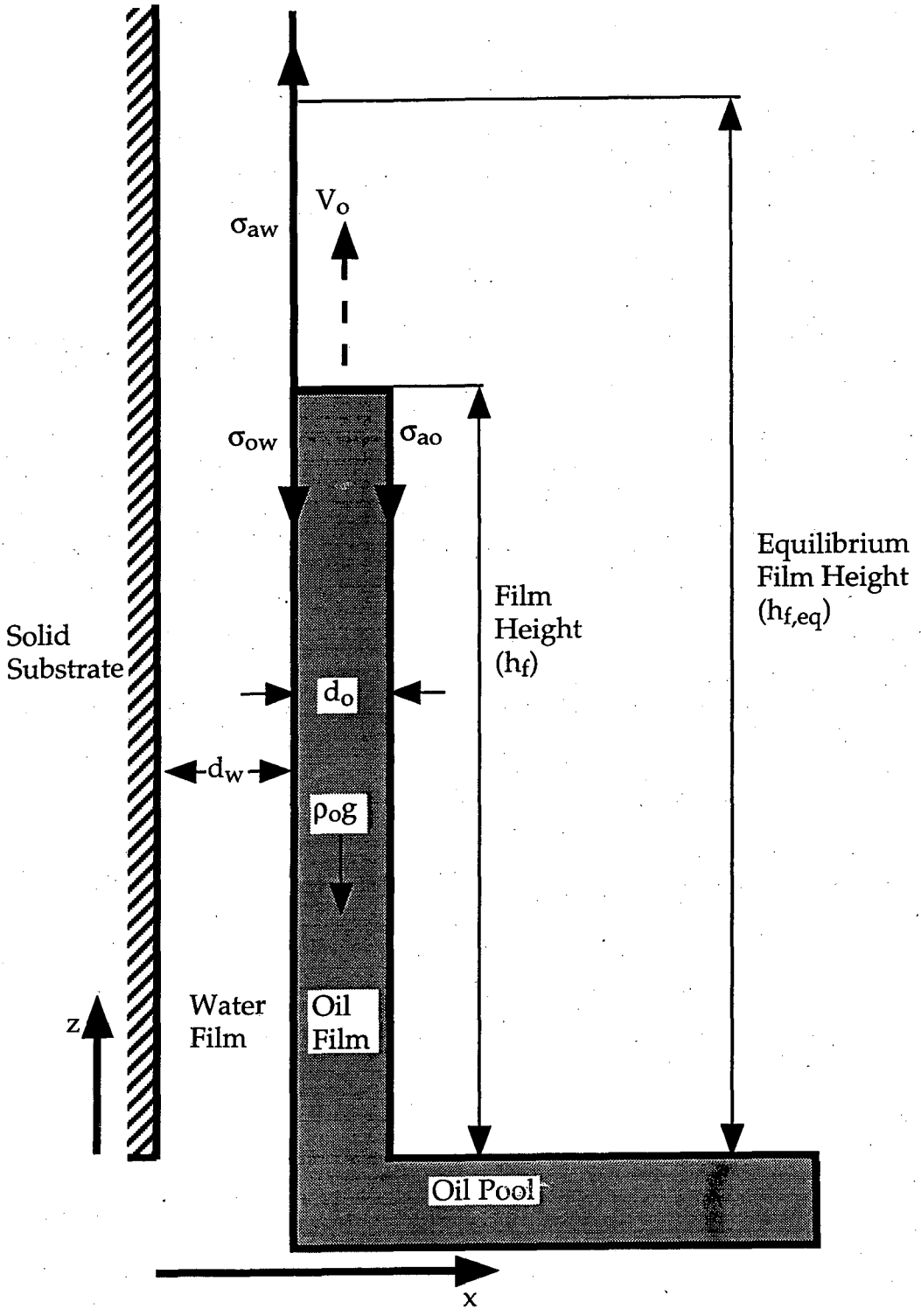

Figure 1. Conceptualization of an oil film spreading vertically over a water film on a solid substrate.

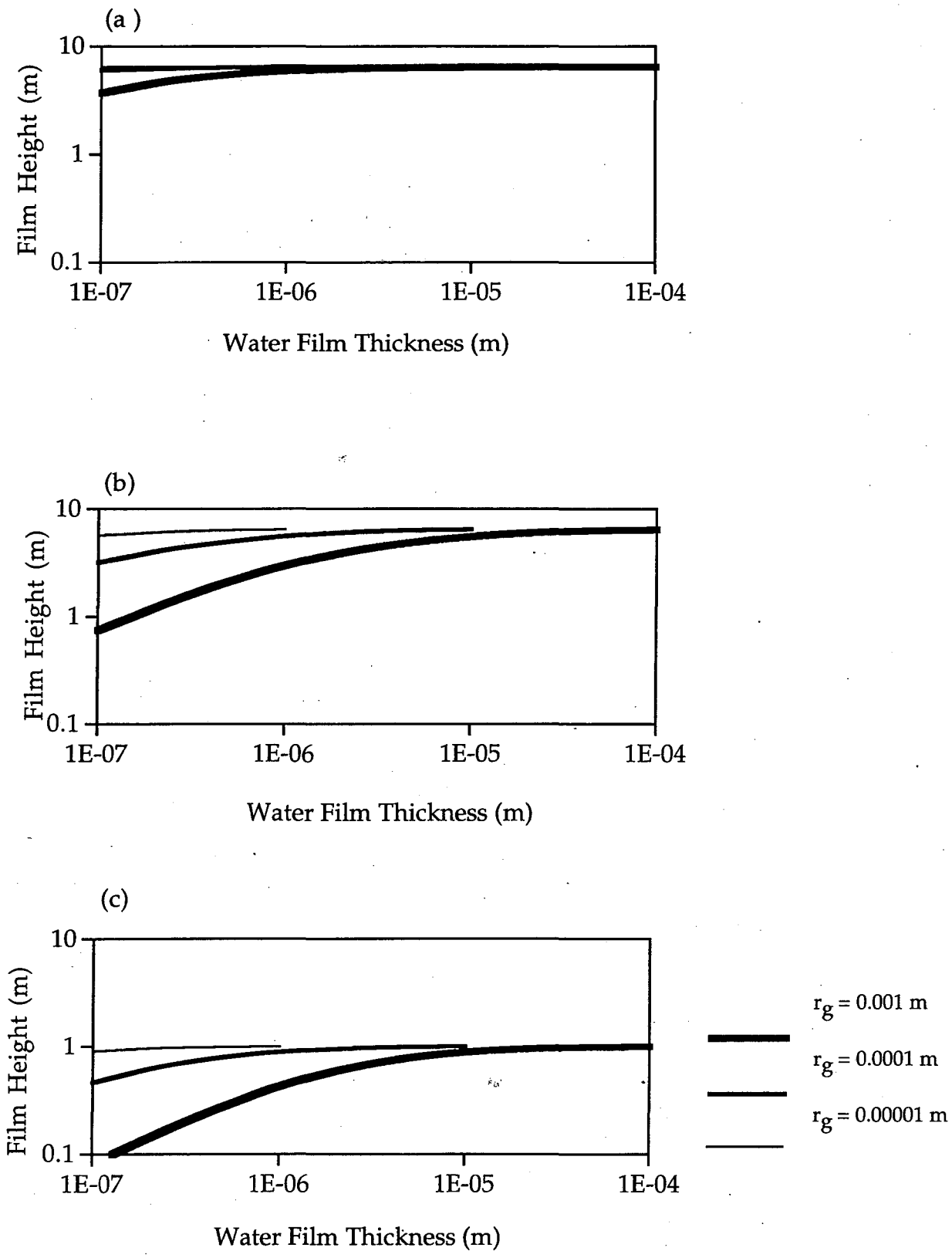

Figure 2. Hexane film height versus water film thickness for vadose zone thicknesses of (a) 100 m, (b) 10 m, and (c) 1 m.

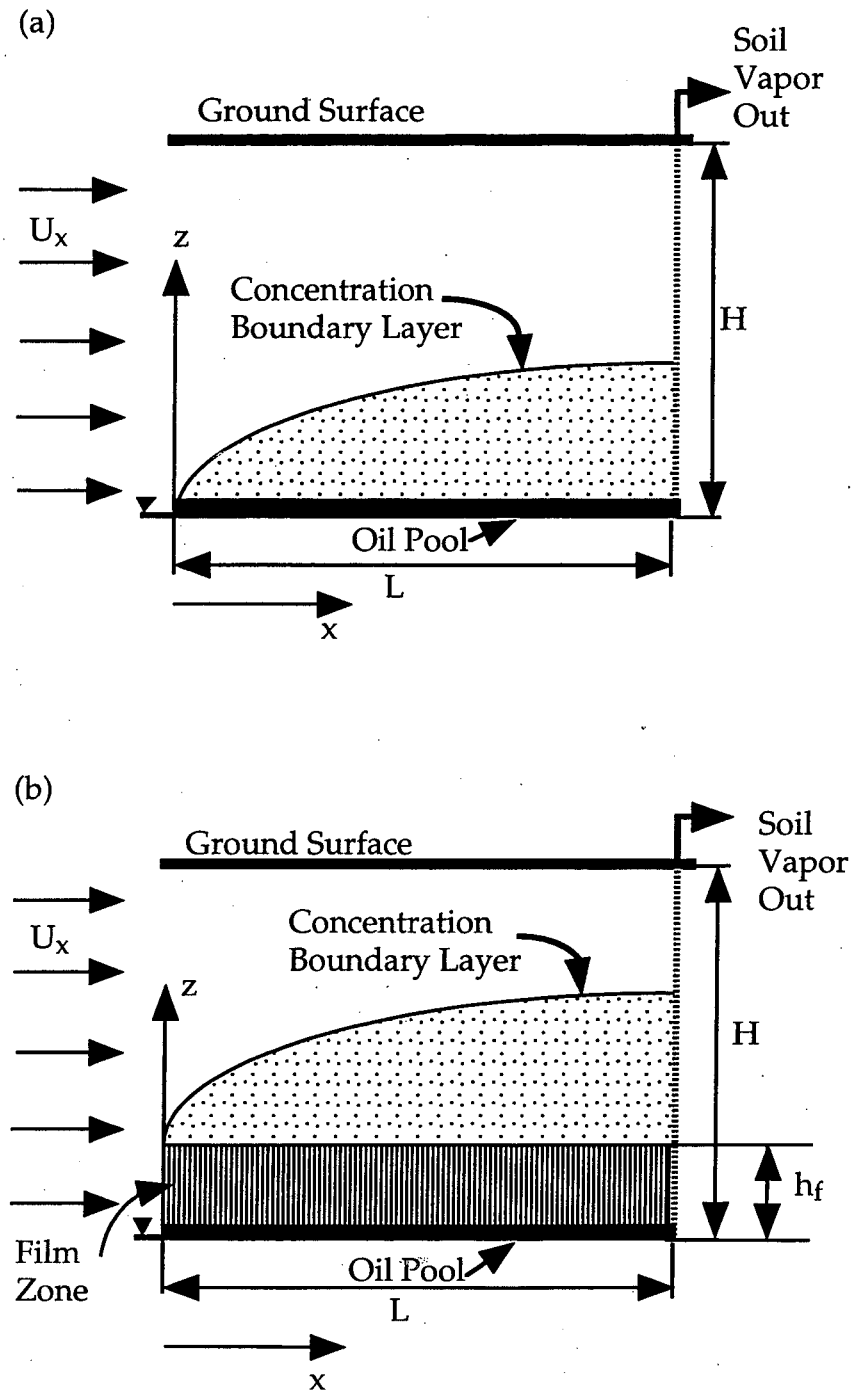

Figure 3. Development of a concentration boundary layer during soil vapor extraction for (a) nonspreading and (b) spreading cases.

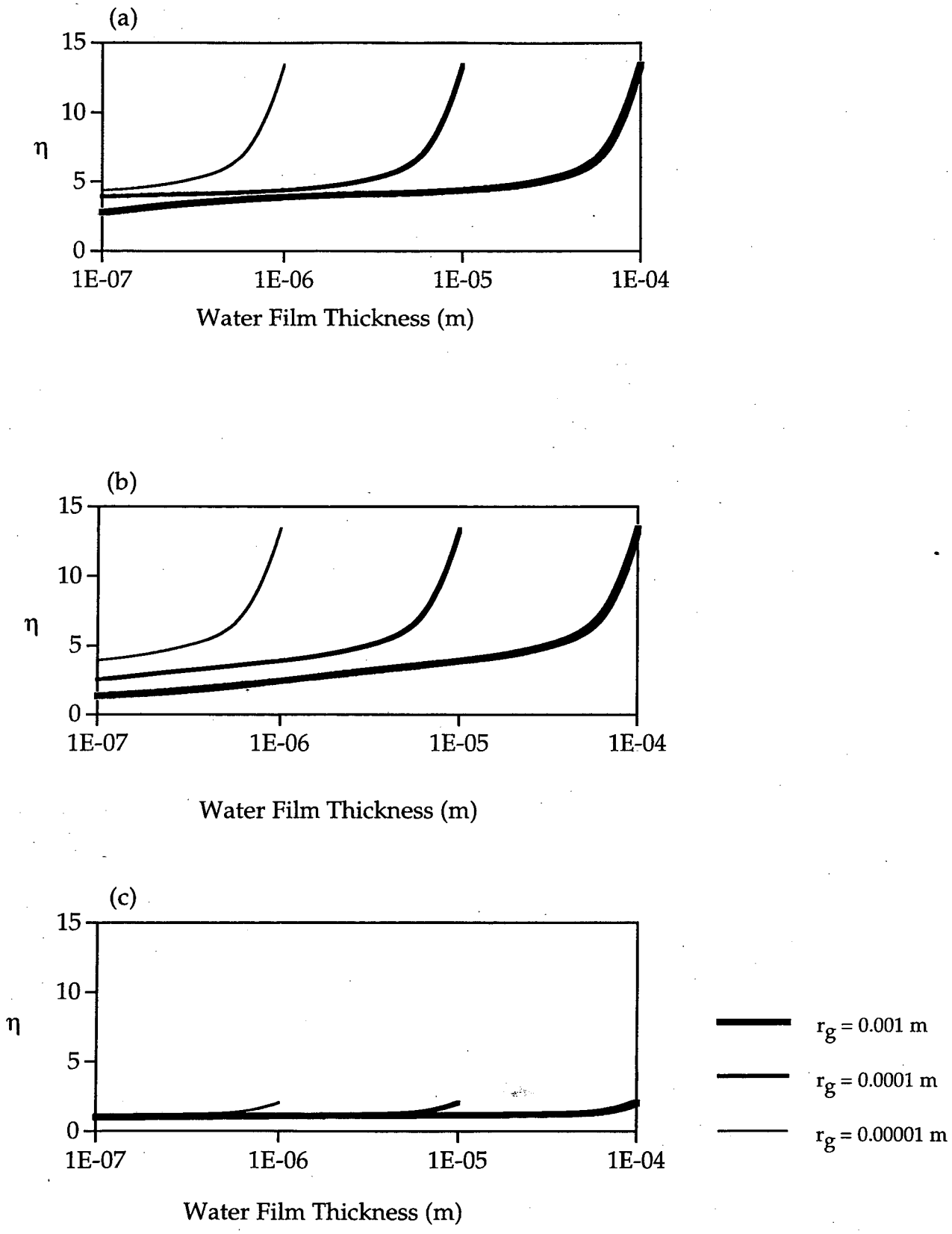

Figure 4. Predicted enhancement factor for hexane recovery comparing spreading and nonspreading conditions as a function of water film thickness for $\alpha = 0$ and vadose zone thicknesses of (a) 100 m, (b) 10 m, (c) 1 m.

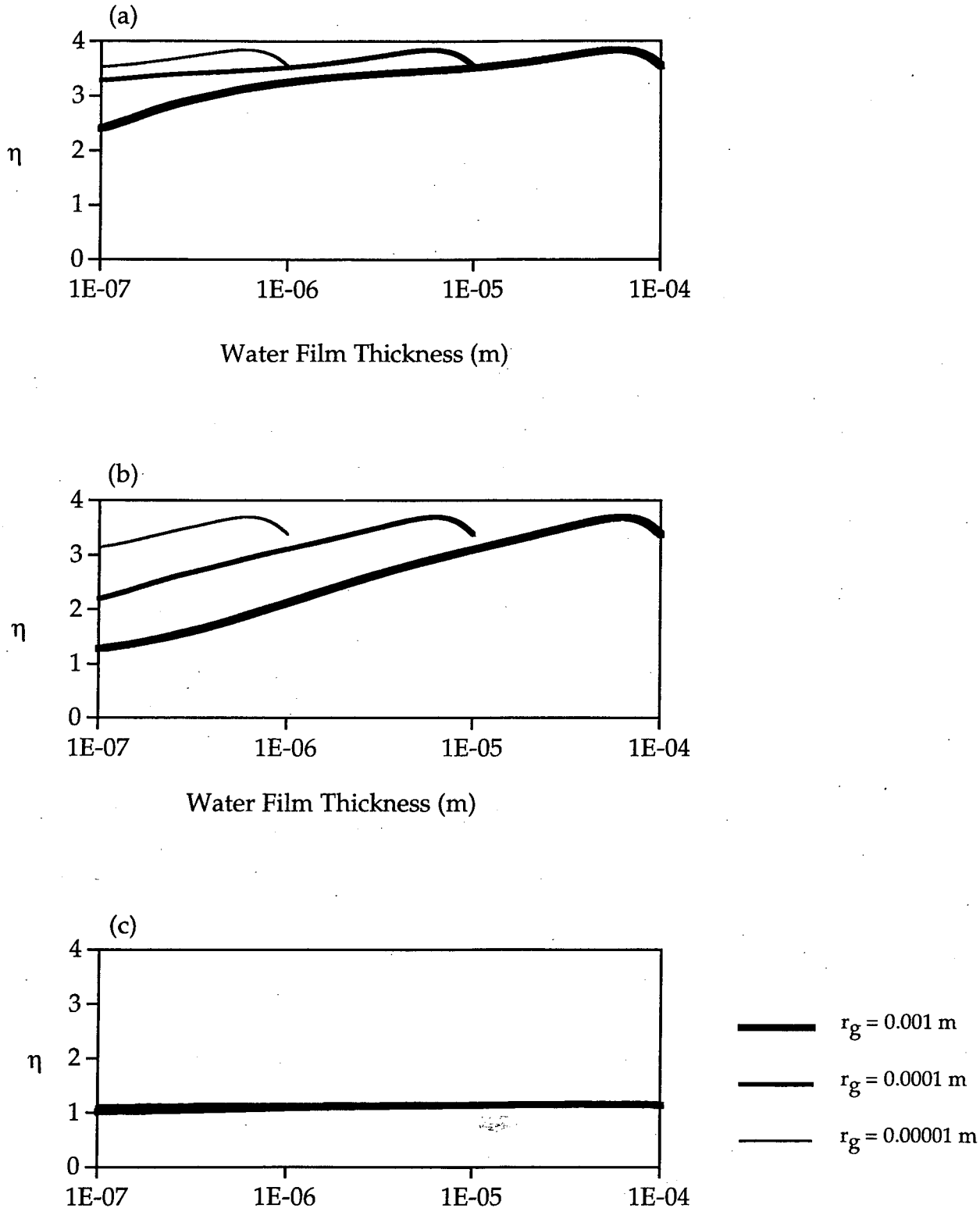

Figure 5. Predicted enhancement factor for hexane recovery comparing spreading and nonspreading conditions as a function of water film thickness for α = 0.039 m for vadose zone thicknesses of (a) 100 m, (b) 10 m, (c) 1 m.

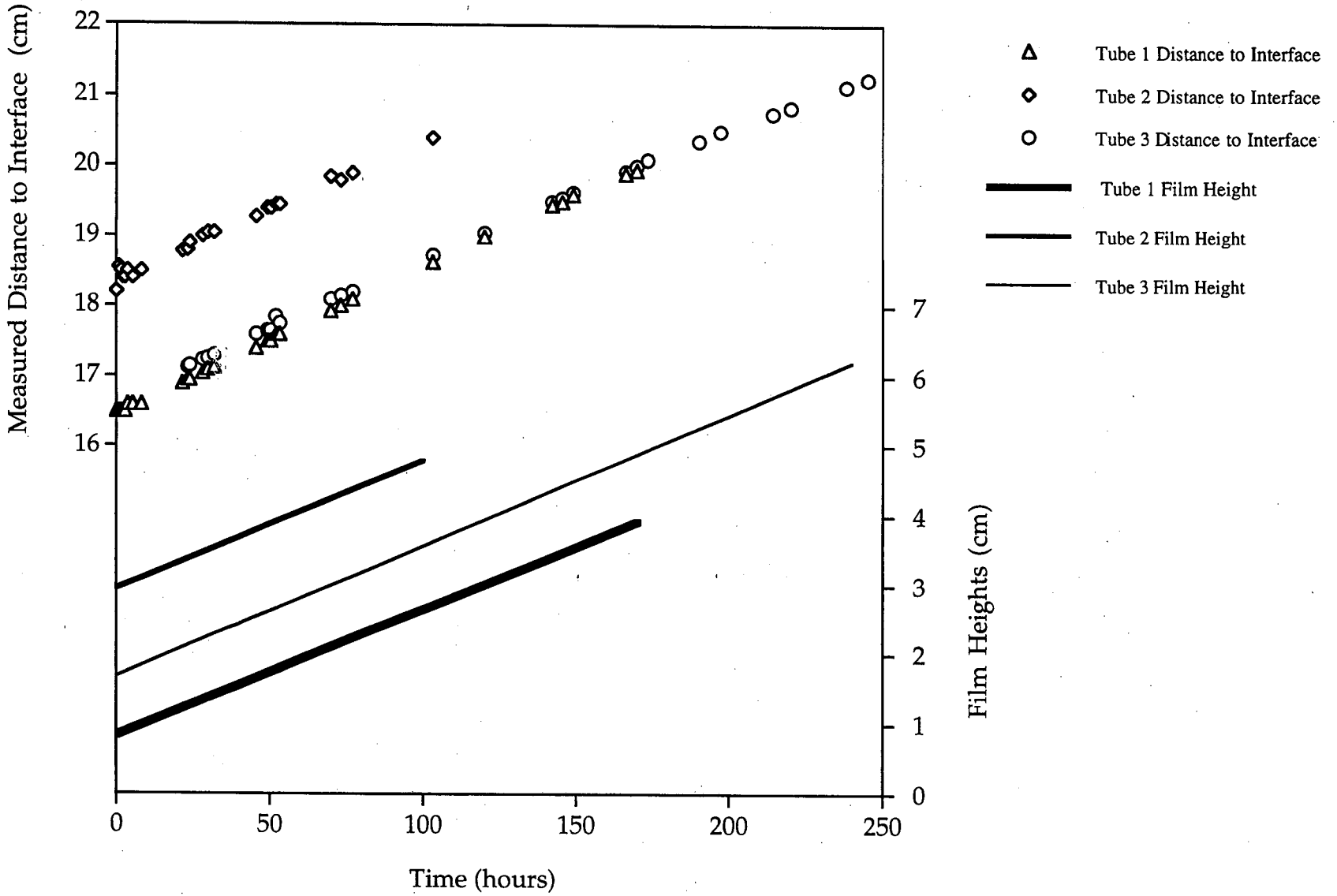

Figure 6. Measured distances to the hexane-air interface and calculated film heights in three capillary tube experiments.

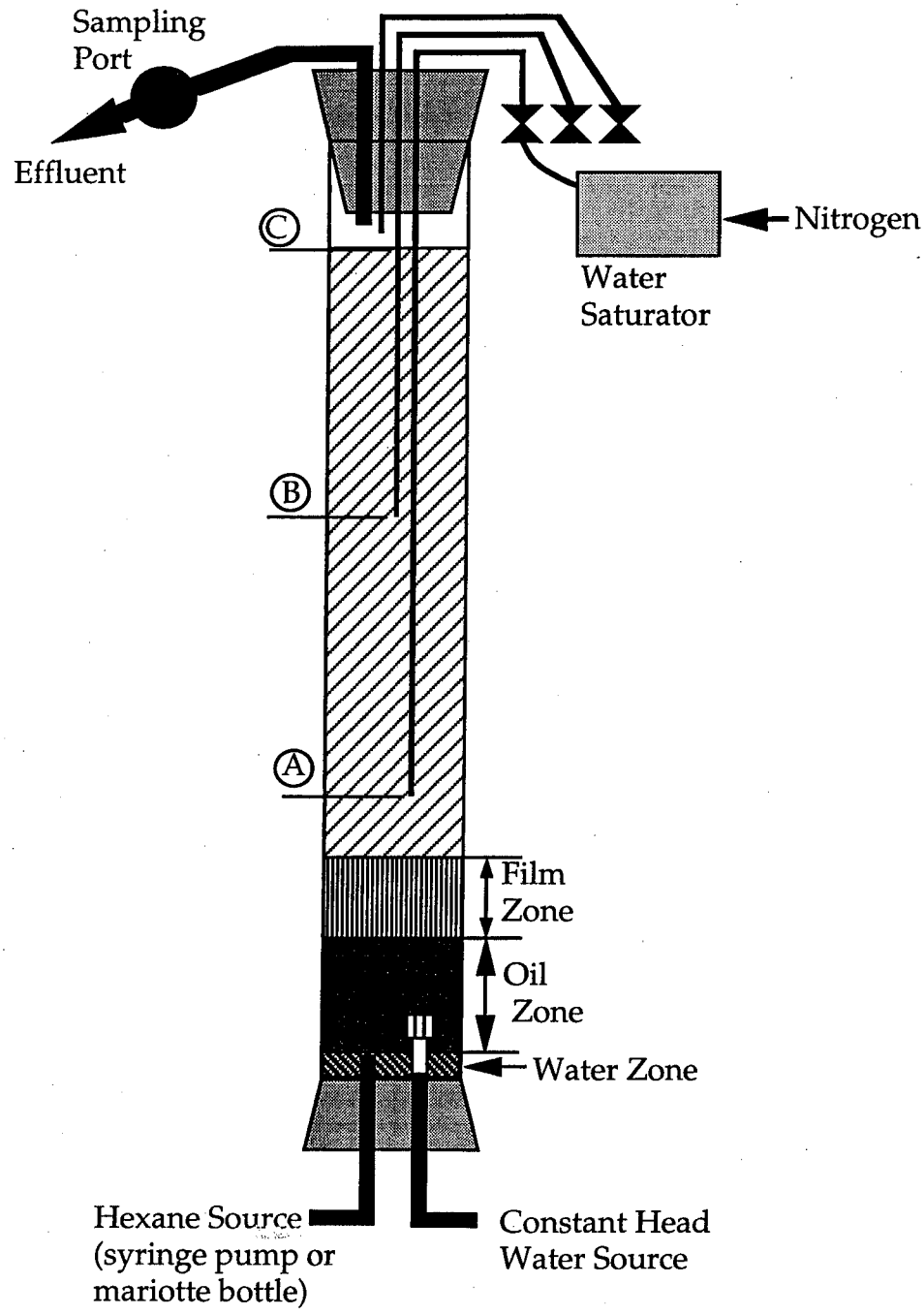

Figure 7. Large-Scale Column Experiment setup.

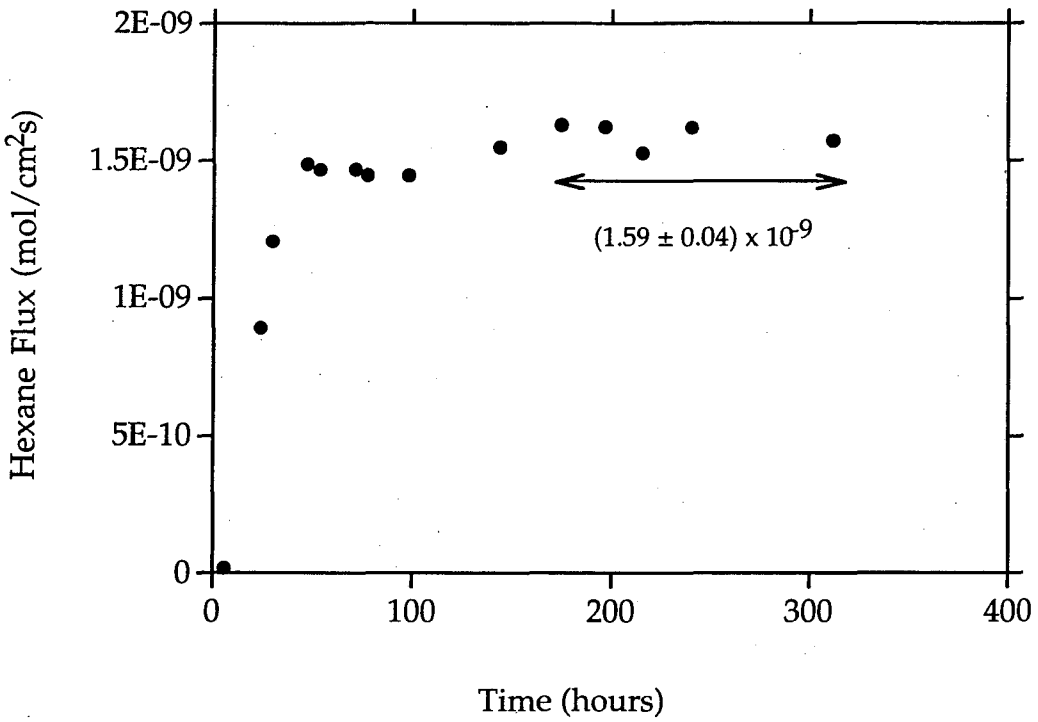

Figure 8. Hexane flux in spreading Experiment 5.

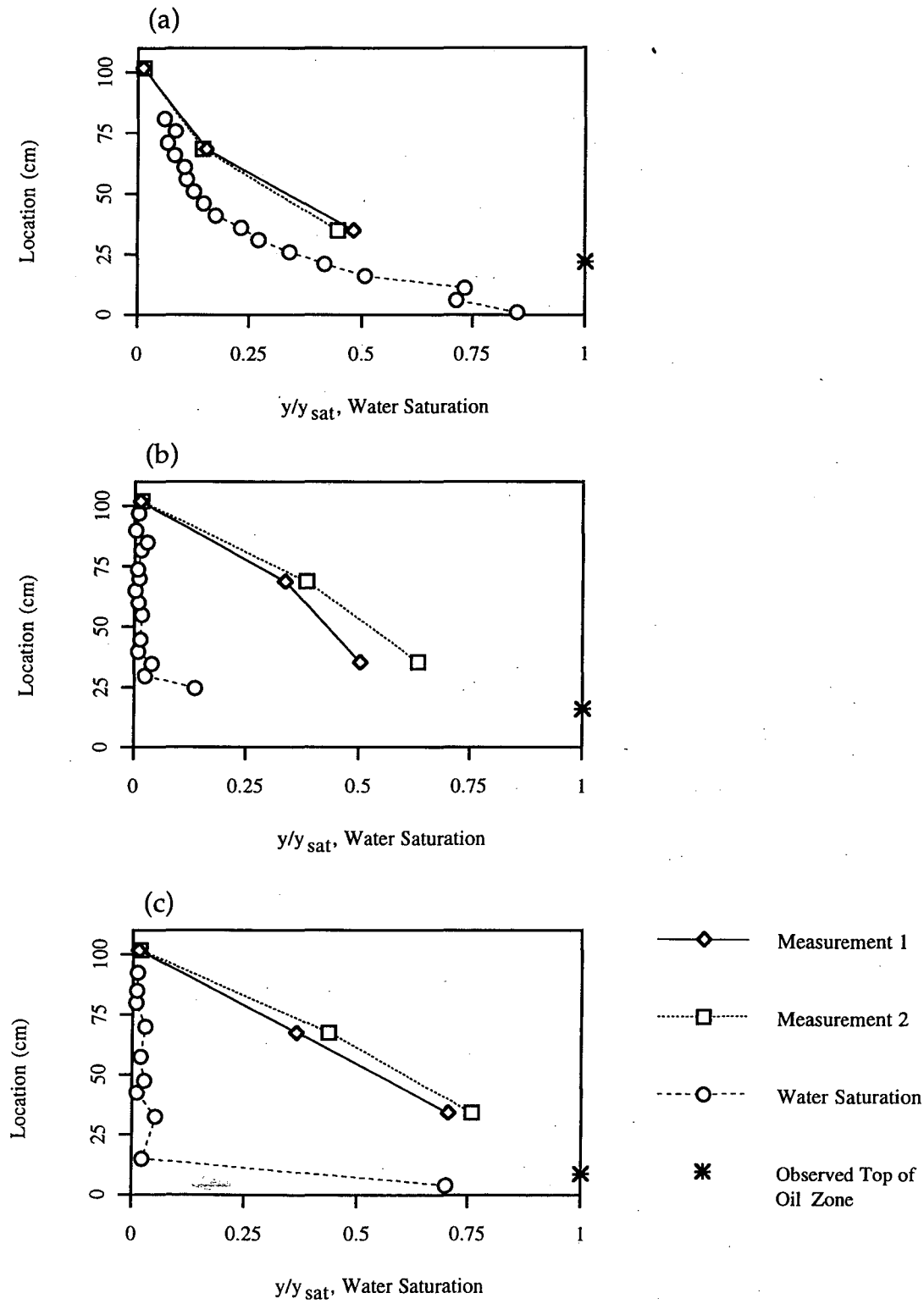

Figure 9. Steady-state hexane relative mole fraction and water content profiles for sweep gas introduced at location C: (a) Experiment 1A, (b) Experiment 2A, (c) Experiment 3A.

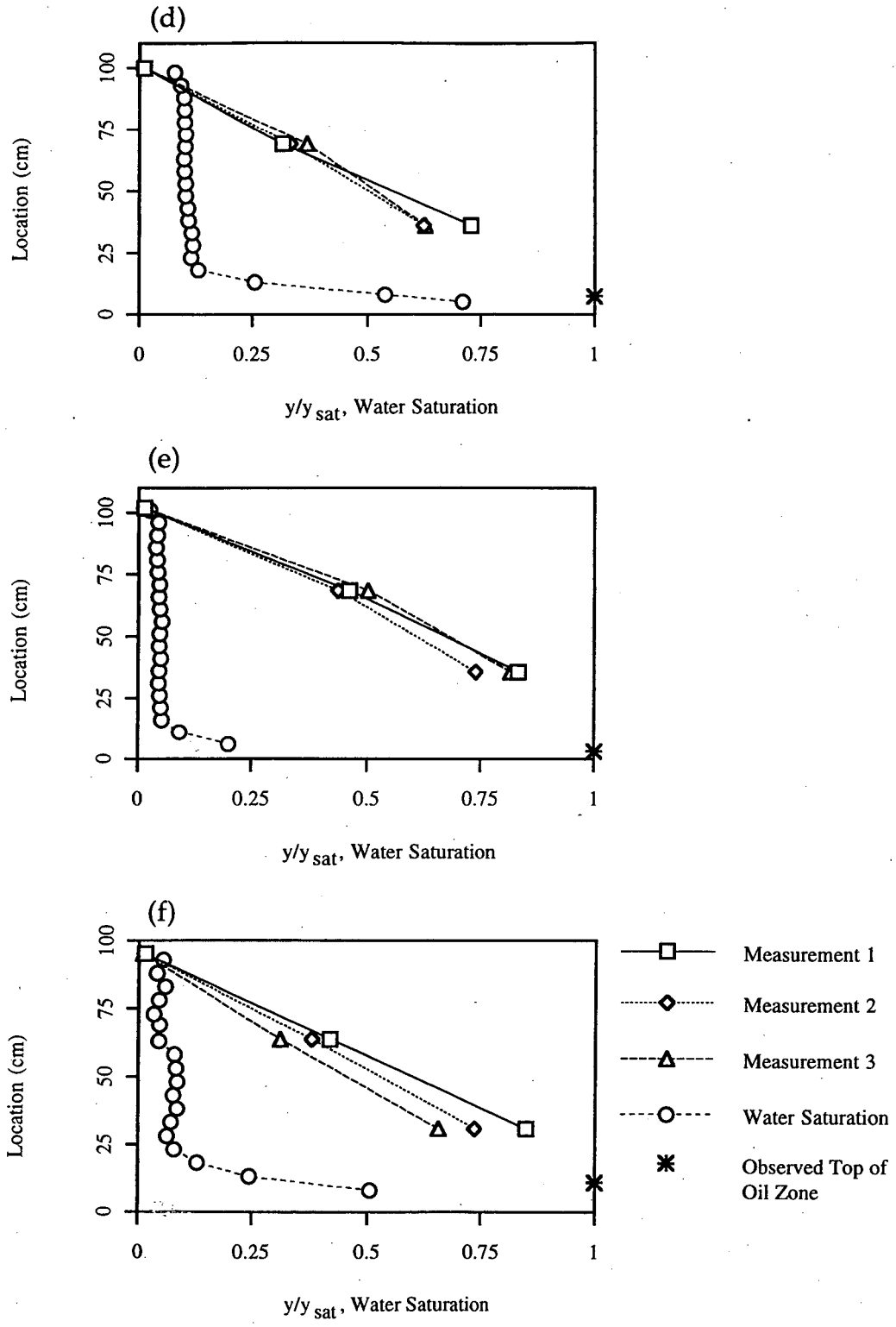

Figure 9 continued. Steady-state hexane relative mole fraction and water content profiles for sweep gas introduced at location C: (d) Experiment 4, (e) Experiment 5, (f) Experiment 6.

Ernest Orlando Lawrence Berkeley National Laboratory
One Cyclotron Road | Berkeley, California 94720

Prepared for the U.S. Department of Energy under Contract No. DE-AC03-76SF00098